J. Appl. Comput. Mech., 9(4) (2023) 1036-1048
DOI: 10.22055/jacm.2023.42512.3935

ISSN: 2383-4536
jacm.scu.ac.ir

Shahid Chamran University of Ahvaz

Journal of Applied and Computational Mechanics

Research Paper

# Fluid-dynamic Simulations for Assessment of Dimensioning Methodologies of Pelton Turbine Buckets Considering the Initial Torque Overcoming

**Jorge Mario Ceballos Zuluaga**[1], **Cesar Augusto Isaza Merino**[1], **Iván David Patiño Arcila**[2], **Andrés David Morales Rojas**[1]

[1] Grupo de Investigación e Innovación en Energía, Facultad de Ingeniería, I.U. Pascual Bravo. Calle 73 # 73A – 226. 050034 Medellín, Colombia
Email(s): j.ceballos728@pascualbravo.edu.co (J.M.C.Z.); c.isaza2059@pascualbravo.edu.co (C.A.I.M.); andres.morales@pascualbravo.edu.co (A.D.M.R.)

[2] Grupo de Investigación e Innovación Ambiental, Facultad de Ingeniería, I.U. Pascual Bravo, Calle 73 # 73A-226, 050034, Medellín, Colombia, Email: i.patinoar@pascualbravo.edu.co

Received December 11 2023; Revised March 30 2023; Accepted for publication April 30 2023.
Corresponding author: I.D. Patiño Arcila (i.patinoar@pascualbravo.edu.co)


**Abstract.** The growing demand for energy resources highlights the need to optimize traditional energy transformation systems. Pelton-type turbines, which are extensively used in micro-generation systems, can be designed using different methodologies, however, no consensus has been reached on which methodology guarantees greater efficiency. This work aims to compare the fluid-dynamic behavior at the first-time instants of Pelton turbines for micro-generation dimensioned by three different methodologies, namely, OLADE, Nechleba, and Thake, evaluating their capacity to overcome the initial torque. The results show that OLADE methodology leads to the best fluid-dynamic performance, whereas Nechleba fails to overcome the prescribed torque. In the Thake methodology, the impact of water on the back face of buckets and the formation of reverse pressure gradients can counter the turbine rotation.

**Keywords:** Computational Fluid Dynamics, Dynamic mesh model, Multiphase flow, Pelton Turbines, Buckets dimensioning methodologies, Initial torque.

## 1. Introduction

Energy resources nowadays known as renewable resources were the very first ones to be harnessed by humankind. However, the rapid development of the modern world allowed the flexibility of fossil and nuclear power technologies at the time, leaving renewable resources aside. These conventional energy resources have gradually produced many problems such as pollution, contaminated waste, depletion of resources, and in many cases strong dependency on imported supplies of some countries. By the year 2019, hydro-energy contributed 2.5 % (15.2 EJ) of the 606 EJ supplied globally. Although hydro-energy appeared less than biomass (9.4 %), it was still higher than other renewable energies like sun and wind (2.2 %). The outlook for the hydro-energy to the year 2040 in the Sustainable Development Scenario (SDS) is that it grows nearly 37.5 %, reaching 24.1 EJ [1]. Many countries rely heavily on hydroelectric power to meet their electricity demands [2]. Due to this, the world begun to reevaluate sustainable and renewable power resources that are competitive with conventional power sources [3]. Over 100 years ago, Pelton-type turbines were developed for harvesting clean energy from water jets with minimal on-site monitoring and carbon-free energy production. These turbines are frequently utilized in locations with significant water flow gradients or where reservoirs can be built to produce the necessary hydraulic head. The Pelton-type turbine consists of four major components: the collector (1), injector (2), buckets and runner (3), and housing (4), as shown in Fig. 1. Over the past 30 years, many researchers [4] have used Computational Fluid Dynamics (CFD) to model reaction turbines. However, modeling Pelton-type turbines remains challenging due to pressure losses, secondary flows, jets, film flow, unsteadiness, and complex interaction between components, among others [5].

For the bucket design of Pelton-type turbines, many sizing methodologies have been studied. These methodologies aim to provide the main formulae and variables to be considered by the designer when dimensioning the injector and buckets under specific operational conditions. For instance, Nechleba [6], Mosonyi [7], Eisenring [8], and Thake [9], among others, have proposed guidelines for buckets design. However much of the experimental data is not publicly available and is retained as a business secret by the turbine manufacturers; therefore, it is typically unknown what kind of studies these standards are based on [10]. However, some recommendations are based on theoretical calculations and suppositions, generally consistent with commercial product designs. Several authors have focused their efforts on analyzing the Pelton-type turbine buckets using computational

Published online: May 05 2023

tools. For instance, Židonis et al. [11] identified the optimum number of buckets in a Pelton-type turbine using CFD. Others authors [12] studied different parameters such as the length, width, depth, height and angle of the splitter, the exit angle, and the bucket attack angle. Additionally, researchers have studied the Pelton-type turbine bucket under stationary and dynamic fluid conditions. For example, in a recent study, three sizing methodologies for the design of Pelton-type turbine buckets were compared based on the ratio of safety factor to bucket weight, and considering equivalent static pressures, obtaining the most suitable bucket design for a specific operational condition [13]. Avellan et al. [14] analyzed free surface flows (FSF) using CFD tools to study the Pelton-type turbine bucket under stationary conditions, and the results of pressure obtained by CFD were compared with experimental results obtained by pressure sensors. Zoppe et al. [15] varied the angle of incidence of the water jet in a Pelton-type turbine bucket to study the pressure generated during the rotation. The results evidenced some agreement with experiments, with errors associated to the flow loss through the cut-out. Klemetsen et al. [16] investigated how the water jet interacts with a stationary bucket using both CFD codes and Fluent, and the numerical results showed acceptable agreement between these methodologies, even when the problem was solved in steady state with CFD codes and transient state with Fluent.

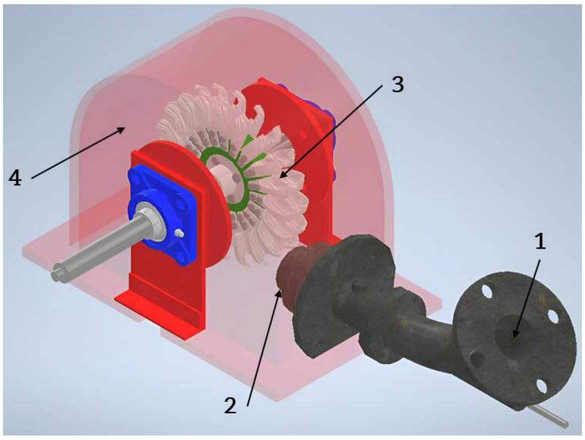


**Fig. 1.** Main components of a Pelton-type turbine.

Similarly, for dynamic conditions, several works have been carried out. To study these conditions, the authors have used the volume of fluid (VOF) method, and the two-phase homogeneous method. For example, Perrig et al. [17] simulated an ideal jet striking on a rotating runner and compared their simulations with experimental data. CFD was used to assess turbulence, and the homogeneous model was used to represent the multiphase flow. The major conclusion of this study was that the k-$\varepsilon$ turbulence model has some issues simulating flow near the cutout region. Xiao et al., [18] used the same model to study the unsteady patterns and torque.

Zeng et al. [19] analyzed a Pelton-type turbine by adopting the three-dimensional transient air-water, two-phase flow simulation approach. The authors studied the interactions between the water jets and buckets, and found that pressure pulsation occurred on the bucket surface with the spreading of water and took up 10%–25% of the water energy. Parkinson et al. [20] modeled a full runner with multi-jet operation and presented results of Finite Element Analysis (FEA) of stress coupled with CFD. The authors concluded that experimental and numerical curves of local pressure on the bucket indicate that the outside of the bucket contributed to the torque; similar results were reported by Perrig et al. [17]. Similar works were also carried out by Hana [21], and Kvicinsky [22]. Other researchers [12, 23], studied the flow inside the Pelton-type turbine bucket using a Fast Lagrangian Solver (FLS), which introduces additional terms in the general equations such as the hydraulic losses and flow spreading; however, the solver has some restrictions detailed in such a work. Finally, Vessaz et al. [24] proposed a strategy to optimize the performance of a Pelton runner based on a parametric model of the bucket geometry, simulations and optimizations.

In the present work, multiphase fluid-dynamics simulations are carried out to evaluate the behavior of Pelton-type turbines at the first-time instants considering three different design methodologies for buckets: OLADE, Nechleba, and Thake. The $\kappa$-$\omega$ turbulence model is considered for the fluid flow modeling, whereas the Volume of Fluid (VOF) method is implemented for the multiphase fluid front tracking. Moreover, the dynamic mesh and 6-DOF methodologies are implemented, which are commonly used in turbomachinery analysis. Therefore, initial torque is prescribed on the shaft, and it is assessed the capacity of the set runner-buckets obtained by each methodology to overcome such initial torque with specific jet operating conditions. The pressure field contours and velocity vectors around the buckets are deemed to illustrate the main differences in the fluid flow behavior between the methodologies evaluated here, and how they affect the time behavior of the rotation angle and angular velocity. Significant differences between the results of OLADE, Nechleba and Thake methodologies are obtained, which are detailed in this manuscript.

## 2. Dimensioning Methodology for Pelton-type Turbine Buckets

To design and size a Pelton-type turbine bucket, it is necessary to calculate the hydraulic power ($P_h$), net head ($H_n$), water flow (Q), specific weight of water ($\gamma$) and the total efficiency ($\eta_T$). Equation (1) illustrates the relationship between these variables:

$$P_h = \gamma Q H_n \eta_T \tag{1}$$

For this purpose, we have selected a water flow of Q = 4.4 l/s (0.0044 m$^3$/s) and a gross head of $H_g$ = 68 m. The net head ($H_n$) can be calculated using Equation (2), in which we assume 10% losses in the pipe system due to the friction, as recommended in [25]:

$$H_n = H_g - 0.1H_g \tag{2}$$

For OLADE and Nechleba methodologies, the total efficiency ($\eta_T$) of the system incorporates the hydro-efficiency ($\eta_h$) and the volumetric efficiency ($\eta_v$), as shown in Equation (3). The hydro-efficiency is a measure of how effective the turbine is at converting the potential energy of the water into mechanical energy, while the volumetric efficiency stands for the turbine ability to utilize the available water flow (ratio of actual volume of water striking the bucket and volume of water supplied to the turbine). The Thake methodology [9] considers another kind of efficiency called roll efficiency $(\eta_r)$, as shown in Equation (4). A total efficiency of 70% is assumed in all cases:

$$\eta_T = \eta_h \eta_v \tag{3}$$

$$\eta_T = \eta_r \tag{4}$$

The jet velocity $(C_0)$ depends on a nozzle velocity coefficient $(k_C)$ that varies depending on the methodology considered, as shown in Equation (5). OLADE and Nechleba methodologies assume a coefficient of $k_C$ = 0.98, while Thake considers a coefficient of $k_C$ = 0.97.

$$C_0 = k_C \sqrt{2gH_n} \tag{5}$$

Then, the jet diameter $(d_0)$ can be calculated from Equation (6):

$$d_0 = \sqrt{\frac{4Q}{\pi C_0}} \tag{6}$$

On the other hand, runner diameter $(D_P)$ depends on the angular velocity ($n$) and speed ratio $(k_U)$, as shown in Equation (7). $k_U$ can be seen in Table 1.

$$D_P = \frac{60 k_U \sqrt{2gH_n}}{\pi n} \tag{7}$$

For this purpose, it is selected $n$ = 1800 rpm and $k_U$ = 0.46. Similarly, the number of buckets (Z) depends on the applied methodology. Thake suggests that, for microgeneration purposes, Z = 20 is a good number of buckets for a Pelton-type turbine; instead, OLADE and Nechleba suggest using Table 1 to estimate Z.

**Table 1.** Number of buckets depending on the Runner diameter/ Jet diameter ratio (OLADE and Nechleba).

| $D_P/d_0$ | $k_U$ | Buckets number | |
|---|---|---|---|
| | | $Z_{min}$ | $Z_{max}$ |
| 15 | 0.471 | 21 | 27 |
| 14 | 0.469 | 21 | 26 |
| 13 | 0.466 | 20 | 25 |
| 12 | 0.463 | 20 | 24 |
| 11 | 0.46 | 19 | 24 |
| 10 | 0.456 | 18 | 23 |
| 9 | 0.451 | 18 | 22 |
| 8 | 445 | 17 | 22 |
| 7.5 | 0.441 | 17 | 21 |

Source: Modified from [26].

**Table 2.** Dimensions and variables of buckets dimensioning under the three methodologies (OLADE, Nechleba and Thake).

| Symbol | OLADE | Nechleba | Thake |
|---|---|---|---|
| | 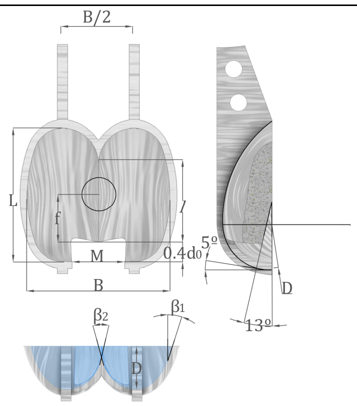 | 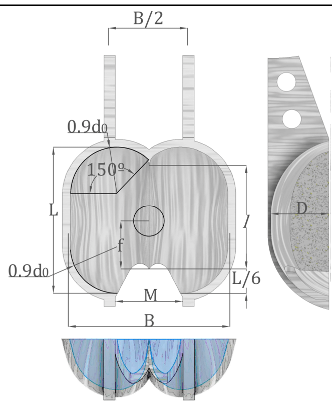 | 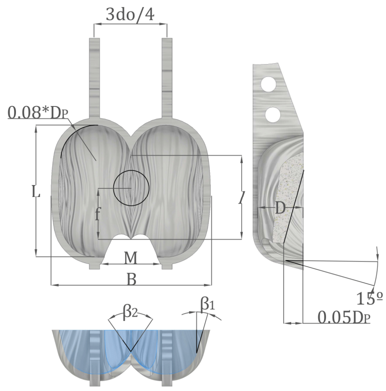 |
| B [mm] | $3d_0$ | $3.2d_0$ | $0.34D_P$ |
| L [mm] | $2.8d_0$ | $2.8d_0$ | $0.30D_P$ |
| D [mm] | $0.9d_0$ | $0.9d_0$ | $0.1D_P$ |
| f [mm] | $0.9d_0$ | $0.9d_0$ | $0.114D_P$ |
| M [mm] | $1.1d_0$ | $1.2d_0$ | $0.14D_P$ |
| l [mm] | $1.6d_0$ | $2d_0$ | $0.184D_P$ |
| $\beta_1$ [°] | 15 | - | 15 |
| $\beta_2$ [°] | 16 | - | 15 |

Source: Modified from [6, 9, 26].

**Table 3.** Results of Parameters for buckets dimensioning.

| Symbol | OLADE | Nechleba | Thake | Symbol | OLADE | Nechleba | Thake |
|---|---|---|---|---|---|---|---|
| $\rho$ [Kg/m$^3$] | | 998 | | $k_U$ [-] | | 0.46 | |
| $g$ [m/s$^2$] | | 9.8 | | $n$ [rpm] | | 1800 | |
| $\gamma$ [N/m$^3$] | | 9780.4 | | $D_P$ [m] | | 0.169 | |
| $H_b$ [m] | | 68 | | T [N.m] | 11.19 | 11.19 | 11.22 |
| $H_n$ [m] | | 61.2 | | B [mm] | 42 | 44.8 | 43.27 |
| Q [m$^3$/s] | | 0.00442 | | L [mm] | 39.2 | 39.2 | 38.18 |
| $\eta_h$ [-] | 0.84 | | - | D [mm] | 12.6 | 12.6 | 12.73 |
| $\eta_v$ [-] | 0.95 | | - | M [mm] | 15.4 | 16.8 | 17.82 |
| $\eta_r$ [-] | - | - | 0.8 | f [mm] | 12.6 | 12.6 | 14.51 |
| $P_h$ [W] | 2109.50 | 2110 | 2114.79 | L [mm] | 22.4 | 28 | 23.42 |
| $k_C$ [-] | 0.98 | | 0.97 | $\beta_1$ [°] | 15 | - | 15 |
| $C_0$ [m/s] | 33.94 | 33.94 | 33.60 | $\beta_2$ [°] | 16 | - | 15 |
| $d_0$ [m] | 0.014 | 0.014 | 0.014 | | | | |

Equation (8) can be used for relating the jet and runner diameters in the Thake methodology, maintaining the proportionality of the buckets. Table 2 shows all dimensions and variables used in the buckets dimensioning with the three methodologies evaluated here.

$$d_0 = 0.11 D_P \tag{8}$$

The Nechleba bucket does not consider angles $\beta_1$ and $\beta_2$. In the present work, all buckets are modeled with a thickness of 1.5 mm, which is a value not usually specified in bucket sizing methodologies and usually depends on the initial impact conditions. Finally, the torque exerted ($T$) by the turbine is estimated from Equation (9):

$$T = \frac{P_h}{n} \tag{9}$$

Table 3 shows the parameters used for the buckets dimensioning with each methodology. The runner or rotor is designed following the geometry of the bucket support.

## 3. Governing Equations and Numerical Models

### 3.1 Multiphase turbulent fluid flow

In the present work, the Volume of Fluid (VOF) and $k$-$\omega$ turbulence models are used to describe the multiphase fluid flow. Therefore, in addition to the continuity equation (10) and momentum equation (11), the interface tracking equation of the VOF model (12), as well as the transport equations for the turbulence kinetic energy (13) and the specific dissipation rate (14), shall be considered. In these equations, the density and viscosity are volume-averaged properties, whereas the velocity field $(\vec{v})$, fluid pressure ($p$), and turbulence quantities ($k$ and $\omega$) are shared among both phases (water and air in this case). The mass transfer per unit volume from phase "$t$" to phase "$q$", and vice-versa, are represented by $\dot{m}_{tq}$ and $\dot{m}_{qt}$, respectively, whereas $n_{ph}$ represents the number of phases, and $\alpha_q$ is the volume fraction of phase "$q$". On the other hand, the source/sink terms of these equations are $S$, $\vec{F}$, $S_{\alpha q}$,$S_k$ and $S_\omega$. In the present case, $S$ and $\vec{F}$ stand for the mass added to the mixture of water/air and the body forces from a dispersed phase, respectively. The source term $\vec{F}$ also considers the surface tension and adhesion effects. In the case of turbomachinery, both $S$ and $\vec{F}$ can be set to zero. Regarding the interface tracking equation (12), the corresponding source term $S_{\alpha q}$ is also set to zero because species transport is not applicable here. The turbulent source parameters $(S_k$ and $S_\omega)$ are considered null as well.

Moreover, the parameters for calculation of the turbulence production terms $(G_k$ and $G_\omega)$, turbulence dissipation terms $(Y_k$ and $Y_\omega)$, and effective diffusivity terms $(\Gamma_k$ and $\Gamma_\omega)$ are kept by default, whereas buoyancy parameters $(G_b$ and $G_{\omega b})$ are set to zero. Accordingly, the solution variables are the mass balance of the mixture, the three components of the velocity vector ($v_x$, $v_y$, and $v_z$), the turbulence quantities ($k$ and $\omega$), and the volume fraction of the secondary phase $(\alpha_{\text{water}})$:

$$\frac{\partial \rho}{\partial t} + \nabla \cdot (\rho \vec{v}) = S \tag{10}$$

$$\frac{\partial (\rho \vec{v})}{\partial t} + \nabla \cdot (\rho \vec{v} \vec{v}) = -\nabla p + \nabla \cdot \left( \mu \left( \nabla \vec{v} + \nabla \vec{v}^T \right) \right) + \rho \vec{g} + \vec{F} \tag{11}$$

$$\frac{\partial}{\partial t}(\alpha_q \rho_q) + \nabla \cdot (\alpha_q \rho_q \vec{v}_q) = S_{\alpha q} + \sum_{t=1}^{n_{ph}} (\dot{m}_{tq} - \dot{m}_{qt}) \tag{12}$$

$$\frac{\partial}{\partial t}(\rho k) + \nabla \cdot (\rho k \vec{v}) = \nabla \cdot (\Gamma_k \nabla k) + G_k - Y_k + S_k + G_b \tag{13}$$

$$\frac{\partial}{\partial t}(\rho \omega) + \nabla \cdot (\rho \omega \vec{v}) = \nabla \cdot (\Gamma_\omega \nabla \omega) + G_\omega - Y_\omega + S_\omega + G_{\omega b} \tag{14}$$

### 3.2 Dynamic mesh and Six-DOF

The dynamic mesh model is very useful in the simulation of turbomachinery since it allows considering the motion of rigid boundaries in the fluid domain; in the present problem, these boundaries are the runner and buckets of the Pelton-type turbine since their strains can be considered very small. In a dynamic mesh, the integral form of the conservation equations (15) is employed:

$$\frac{d}{dt}\int_{V}\rho\varphi dV+\int_{\partial V}\rho\varphi\left(\vec{v}-\vec{v}_g\right)\bullet d\vec{A}=\int_{\partial V}\Gamma\nabla\varphi\bullet d\vec{A}+\int_{V}S_{\varphi}dV \tag{15}$$

with $\varphi,\rho,\vec{v},\vec{v}_g,\Gamma$ and $S_\varphi$ as the conservation scalar quantity (mass, velocity component, turbulence quantities, and volume fraction), fluid density, flow velocity vector, mesh velocity vector, diffusion coefficient, and source term, respectively. The inertial term of equation (15) can be approximated using a first-order or second-order backward scheme, where the time derivative of the control volume is computed by equation (16):

$$\frac{dV}{dt}=\int_{\partial V}\vec{v}_g\cdot d\vec{A}=\sum_{j}^{n_f}\vec{u}_{g,j}\cdot\vec{A}_j \tag{16}$$

where $n_f$, $\vec{u}_{g,j}$ and $\vec{A}_j$ are the number of faces of the control volume, average velocity of the face "j" and area vector of the face "j", respectively. Considering a rigid moving boundary, the values of $\vec{u}_{g,j}$ can be determined from the translational and rotational motion of the enclosed domain, which can be described by the equations (17) and (18) according to the 6-DOF methodology:

$$\dot{\vec{V}}_G=\frac{1}{m}\sum\vec{f}_G \tag{17}$$

$$\dot{\vec{\omega}}_G=L^{-1}\left(\sum\vec{M}_B-\vec{\omega}_B\times L\vec{\omega}_B\right) \tag{18}$$

where:

$\vec{V}_G$ : Velocity vector of the center of gravity of the enclosed domain.
$m$ : Mass of the enclosed domain.
$\vec{f}_G$ : Force vector at the center of gravity of the enclosed domain.
$\vec{\omega}_B$ : Angular velocity vector of the enclosed domain.
$L$ : Inertia tensor.
$\vec{M}_B$ : Moment vector of the enclosed domain in the body coordinates.

The moment vector in body coordinates, $\vec{M}_B$, is related with such in inertial coordinates, $\vec{M}_G$, by the following equation:

$$\vec{M}_B=R\vec{M}_G \tag{19}$$

where the rotation transformation matrix is given by:

$$R=\begin{bmatrix} C_\theta C_\psi & C_\theta S_\psi & -S_\theta \\ S_\phi S_\theta C_\psi - C_\phi S_\psi & S_\phi S_\theta S_\psi + C_\phi S_\psi & S_\phi C_\theta \\ C_\phi S_\theta C_\psi + S_\phi S_\psi & C_\phi S_\theta S_\psi - S_\phi C_\psi & C_\phi C_\theta \end{bmatrix} \tag{20}$$

where $C_i = \cos(i)$ and $S_i = \sin(i)$, with $i=[\phi,\theta,\psi]$ as the Euler angles. In the present work, a one-DOF rotation is configured for the domain enclosed by the boundaries defined by the set runner-buckets (see Fig. 2b), aiming to emulate the rigid motion of the Pelton-type turbine. Therefore, the mass, inertia moment, center of rotation, axis of rotation, and starting torque (pre-torque) need to be specified.

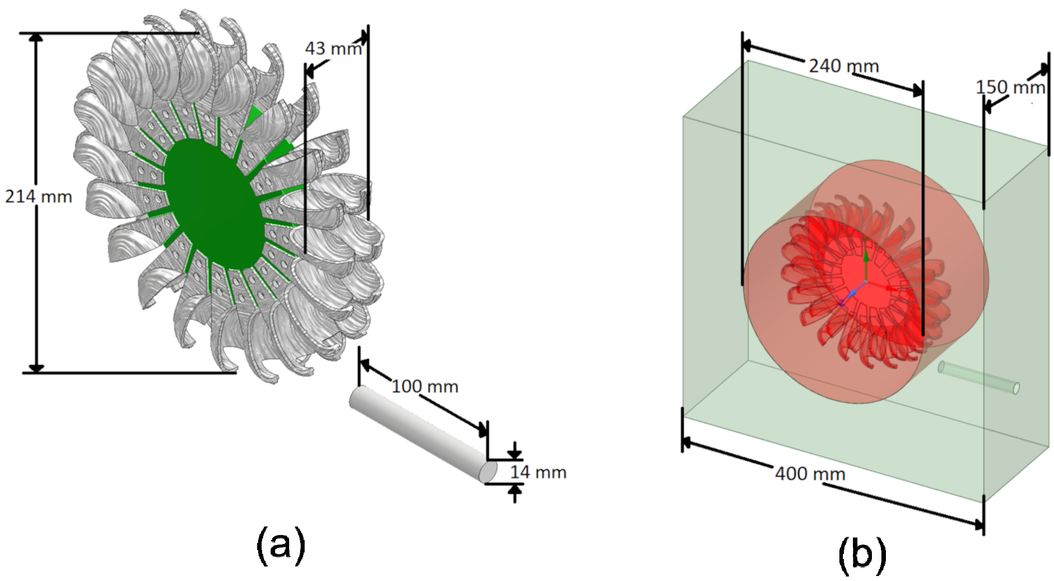


**Fig. 2.** General dimensions for (a) Solid domains and (b) Fluid domains.

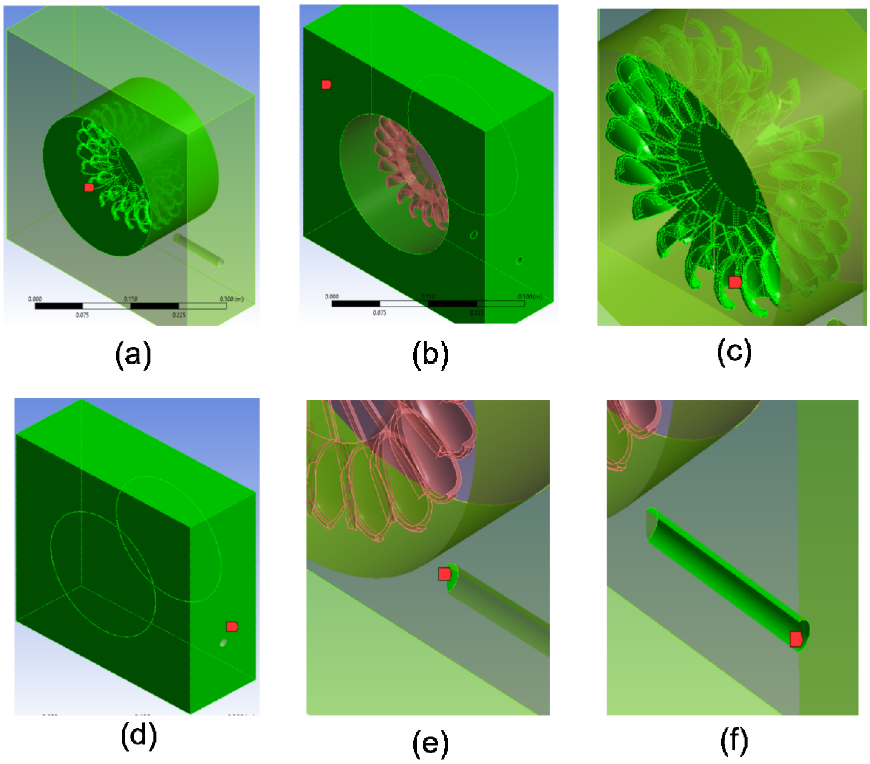

Fig. 3. Definitions of volume and boundary zones. (a) Mobile domain, (b) Static domain, (c) Runner-buckets boundary, (d) Outlet boundary, (e) Inlet boundary, (f) Wall boundary.

## 4. Model Preparation and Simulation Setup

### 4.1 Geometrical modeling and material definition

The computer-aided design software SpaceClaim™ is used to model and prepare the physical domains for the numerical simulations. Firstly, the assembly runner-buckets is drawn as shown in Fig. 2a, then, two fluid enclosures are generated as shown in Fig. 2b. The red-colored enclosure corresponds to the mobile control volume surrounding the set runner-buckets, whose mesh remains unaltered during the whole simulation, whereas the green-colored enclosure is the static control volume that includes the inlet jet and has a deforming mesh. Shared topology is enabled between both sub-domains to bring about a conforming interface mesh. For the present application, the final fluid domain surrounding the set runner-buckets is large enough to guarantee a zero-outlet pressure condition at the external boundaries (see dimensions in Fig. 2b).

### 4.2 Mesh setup and zones definition

For the configuration of the Six-DOF model, two volume and one boundary definitions are created, namely, Mobile-domain (Fig. 3a), Static-domain (Fig. 3b), and Buckets-runner (Fig. 3c). Moreover, the imposition of the boundary conditions implies the definitions of other boundaries: the Outlet boundary representing the limits of the enclosure domain where air pressure is atmospheric (Fig. 3d), the Inlet boundary representing the water jet entrance (Fig. 3e), and the Wall boundary for the jet pipe (Fig. 3f).

A tetrahedral-dominant mesh was used, with the sizing controls and their respective behaviors shown in Table 4. As can be appreciated, finer elements are required in the faces of the buckets given their geometric complexity regarding other zones. Five inflation layers with smooth transitions are imposed at the boundary defined by the set runner-buckets. The meshing statistics generated for all dimensioning methodologies are shown in Table 5.

**Table 4.** Mesh configuration.

| | Volume zones | | Boundary zones | | |
|---|---|---|---|---|---|
| Mesh Controls | Static domain | Mobile domain | Inlet boundary | Runner boundary | Buckets boundary |
| Element Type | Tetrahedrons | | | | |
| Element Size | 6e-3 m | 6e-3 m | 3e-3 m | 3e-3 m | 1e-3 m |
| Behavior of element size | Soft | Soft | Soft | Hard | Hard |

Note: Boundary meshing controls are set as Hard, which means that meshing algorithms prioritize these controls indenting to respect the prescribed element size. For the volume meshing, soft control is selected in such a way that the element size can be recursively affected by proximity, curvature and local re-meshing in order to improve the mesh quality.

**Table 5.** Meshing Statistics.

| | OLADE | Nechleba | Thake |
|---|---|---|---|
| Elements | 5,627,502 | 5,777,254 | 5,699,967 |
| Nodes | 1,536,788 | 1,608,004 | 1,571,506 |

**Table 6.** Mesh Quality Metrics Based on Skewness.

| Skewness values | Classification |
|---|---|
| 0 | Ideal |
| > 0 - 0.25 | Excellent |
| 0.25 - 0.5 | Very Good |
| 0.5 - 0.8 | Good |
| 0.8 - 0.95 | Acceptable |
| 0.95 - 0.98 | Bad |
| > 0.98 – 1 | Unacceptable |

Modified from [27,28].

**Table 7.** Boundary conditions used for the CFD simulations.

| Boundary | Type | Value | Additional characteristics |
|---|---|---|---|
| Inlet of water jet (Fig. 3e) | Inlet velocity | 33.94 m/s | Turbulence intensity: 5%<br>Hydraulic diameter: 14 mm<br>Volume fraction of water: 1 |
| Outlets of the fluid enclosure (Fig. 3d) | Pressure Outlet | Gauge pressure: 0 Pa | Backflow turbulent intensity: 5%<br>Backflow turbulent viscosity ratio: 10<br>Backflow volume fraction of water: 0 |
| Walls of set runner-buckets (Fig. 3c)<br>Walls of jet pipe (Fig. 3f) | Stationary and non-slip wall | Not applied | *Wall roughness:* Standard model with roughness coefficient of 0.5.<br>In the set runner-bucket, the wall condition should be configured as stationary since this set does not induce a velocity field on the multiphase fluid with a prescribed rotational motion; contrarily, the water jet generates a rigid boundary motion on this set, which is estimated with the Dynamic mesh/ 6 DOF methodology. |

The mesh quality analysis is accomplished using the skewness metric, whose classification is shown in Table 6. Fig. 4 shows the histogram of mesh skewness of each methodology, indicating a suitable quality for most of the Tet4 and Wed6 elements according to the range of Table 6. As can be noticed, most of the elements can be categorized in the classification from ideal to good.

### 4.3 Simulation setup for the fluid domain

Incompressible air and water are assigned as the primary and secondary phases, respectively, the surface tension effects are neglected, but gravitational ones are considered. At the inlet boundary (Fig. 3e), an absolute velocity of 33.94 m/s is assigned, which is computed from equation (5) considering a net hydraulic head of $H_n = 61.2\ m$ and a flow rate of Q = 4.4 *l/s* (0.0044 m$^3$/s). The turbulent intensity is set to 5%, and the hydraulic diameter is specified as the jet diameter ($d_o$=14 mm). The volume fraction of the water phase is set to one at this inlet boundary. On the other hand, a zero-gauge pressure is deemed at the outlet boundary of the fluid enclosure (Fig. 3d), whereas no slip, stationary wall conditions are imposed at the remaining boundaries, namely, runner-buckets (Fig. 3c) and wall of jet pipe (Fig. 3f). The summary of the boundary conditions used in the present work is presented in Table 7.

The dynamic mesh configuration includes selecting the mesh settings motion methods, the configuration of the Six-DOF model, and the creation of dynamic mesh zones. In the first case, the three groups of volume mesh updating available in ANSYS Fluent are considered for the deforming mesh of the static domain, namely, smoothing, layering and remeshing. The combination of these three options allows keeping the number of nodes and cells, as well as their connectivity, as mesh deformation takes place, except at the interface between the static and mobile domains, where adjacent cells can be added or removed depending on their height, and/or when the predefined cell quality criterion (maximum skewness) is not fulfilled, in which case cells can be recursively merged or divided. The principal parameters of the smoothing, layering and remeshing operations are shown in Table 8.

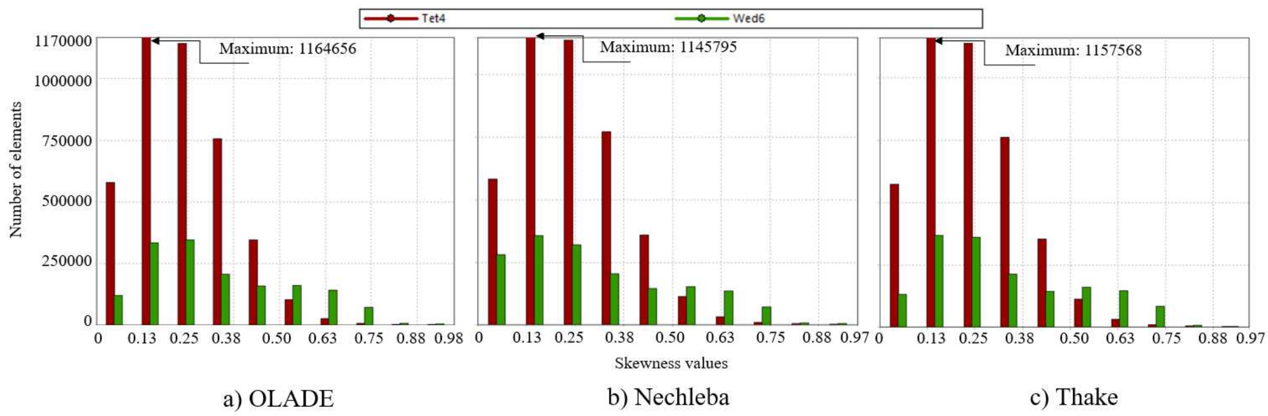


**Fig. 4.** Mesh skewness for the three methodologies considered. (a) OLADE, (b) Nechleba, (c) Thake.

**Table 8.** Principal parameters of smoothing, layering and remeshing operations.

| | Dimensioning methodology | | |
|---|---|---|---|
| | OLADE | Nechleba | Thake |
| Remeshing method and sizing option | Local cells in each interval | | |
| | Length scale interval = 0.000369 to 0.009306 | Length scale interval = 0.00037 to 0.009306 | Length scale interval = 0.00029 to 0.009306 |
| | Max. Cell Skewness = 0.8976 | Max. Cell Skewness = 0.8955 | Max. Cell Skewness = 0.8969 |
| Smoothing method | Diffusion with default advanced parameters | | |
| Layering method | Height based with Split Factor = 0.2 and Collapse Factor = 0.2 | | |

**Table 9.** Input parameters in the Six-DOF model.

| Input parameter | Dimensioning methodology | | |
|---|---|---|---|
| | OLADE | Nechleba | Thake |
| Mass of set runner-buckets [Kg] | 1.276 | 1.273 | 1.248 |
| Moment of inertia of set runner - buckets [Kg.m$^2$] | 0.00437 | 0.0043 | 0.00432 |
| Pre-torque [N.m] | 12.31 | 12.31 | 12.31 |

Note: Pre-torque is calculated from equation (9).

**Table 10.** Main characteristics of the solver.

| Characteristic | Variable | Numerical technique |
|---|---|---|
| Pressure - Velocity Coupling | Scheme | Coupled |
| Transient formulation | Time | Second Order Implicit |
| Spatial discretization | Gradient | Least Squared Cell-Based |
| | Pressure | PRESTO! |
| | Momentum | Second Order Upwind |
| | Volume Fraction | First Order Upwind |
| | Turbulent Kinetic Energy | Second Order Upwind |
| | Specific Dissipation rate | First Order Upwind |

The second step is the configuration of the Six-DOF model. Data for this configuration for each dimensioning methodology of the buckets are shown in Table 9. To complete the dynamic mesh configuration, three dynamic mesh zones are created: the Bucket-runner boundary where the one-DOF rotation is applied, Mobile-domain where a rigid body motion is applied following the moving boundary (bucket-runner), and the Static-domain where the mesh deformation takes place.

The main characteristics of the solver are summarized in Table 10. Under-relaxation is implemented as shown in the following equation:

$$\varphi_{new} = \varphi_{old} + f\left(\varphi_{intermediate} - \varphi_{old}\right) \tag{21}$$

where $\varphi_{new}, \varphi_{old}$ and $\varphi_{intermediate}$ are the updated, current, and intermediate values of the field variables, whereas $f$ is the under-relaxation factor, which is taken as $f = 0.75$ for these transient simulations.

The configuration for running calculations is the same for all methodologies, with a time step size of $\Delta t = 0.001$ s, 47-time steps, and a maximum iteration number of 100 per time step.

## 5. Results and Discussion

### 5.1 Time behavior of rotation angle

Figure 5 shows the time behavior of the rotation angle, $\theta$, obtained from CFD simulations for the three dimensioning methodologies considered here (OLADE, Nechleba, and Thake), with a prescribed initial torque of 12.31 N.m. At the beginning, the change of $\theta$ with the time is very small for all methodologies, however, significant changes become perceptible from t = 1 x $10^{-2}$ s, approximately, which can be considered as the approximate time when the total torque generated by the fluid over the buckets just exceeds the prescribed pre-torque of 12.31 N.m. According to Zeng et al. [29] who used CFD simulations, under normal operating conditions, once this pre-torque is surpassed, the turbine starts moving, impact forces over the buckets decrease, and the angular velocity should rise until it reaches a stable value when turbine is operating in appropriate conditions. Both the prescribed initial torque overcoming and the subsequent behavior of the turbine rotation at the first-time instants are highly influenced by the bucket dimensions and shape. In OLADE, the slope of the curve increases with time, and the final rotation is $\theta = 30.65$ ° at $t = 4.70$ x $10^{-2}$ s; an increasing slope is advantageous because it means that the angular velocity can usually reach a larger nominal value. In Thake, the rotation angles, $\theta$, are smaller than in OLADE as the time evolves, and the slope of the curve tends to reach a zero value, so at the same final time instant (t = 4.70 x $10^{-2}$ s), the final rotation angle is smaller, $\theta$ = 7.79°, indicating a lower angular velocity than in OLADE. In the following sections, these differences between OLADE and Thake results are explained by considering the pressure field contours and velocity vectors over the buckets' surfaces, as well as analyzing the multiphase fluid pressure surrounding the set runner-buckets at the mid-longitudinal plane. On the other hand, the Nechleba case can be considered critical since the $\theta$ vs t curve shows that the initial torque is not overcome for the operating conditions specified here; this case is discarded in the following analyses.

### 5.2 Pressure contours on buckets' surfaces

Figure 6 presents the pressure contours over the buckets' surfaces obtained by the OLADE and Thake methodologies, where sign "P" stands for the bucket struck by water jet and "S" stands for the subsequent bucket in the rotation direction. A different behavior between OLADE and Thake can be observed in terms of the pressure distribution and motion. As has been numerically demonstrated by some authors [29, 30], pressure contours on the buckets at the first-time instants are of particular interest since they determine the highest impact forces exerted by the fluid during the Pelton-type turbine operation. This is not only relevant for the structural design of the buckets, but also for analyzing the turbine capacity to overcome the initial torque. The jet-bucket interaction starts when the first particle trajectories impinge on the notch cut at the front edge of the bucket at relatively small angles. For OLADE methodology, a concentrated pressure in the front part of cavities is noticed (Fig. 6a), while the bucket designed with the Thake methodology shows a pressure distribution tending to the front cutting edge and the rear part of the cavity (Fig. 6b). The concentration of pressure in the front part of the cavities of OLADE buckets allows the Pelton-type turbine based on this methodology to rotate faster than the turbine based on the Thake methodology, which is coherent with results obtained in Fig. 5. This behavior is more evident at the final time instant, t = 4.70 x $10^{-2}$ s, where the rotation angles are $\theta$ = 30.65° for OLADE (Fig. 6e,g) and $\theta$ = 7.61° for Thake (Fig. 6f,h). A similar finding was observed in a previous study [30], where a Computational Fluid Dynamics (CFD) analysis of Pelton-type turbines for predicting the flow behavior was presented. The authors concluded that for optimal performance, the pressure distribution should be maximum at the front part of the bucket and the runner pitch circle diameter. This behavior allows converting most of the hydraulic energy into mechanical energy when the jet strikes the runner pitch circle diameter [17]. However, as previously mentioned, the Thake methodology shows an important pressure distributed over the rear part of the cavities; additionally, there is considerable pressure on the back faces of the subsequent bucket "S" for this methodology, which does not allow the conversion of a significant portion of the hydraulic energy into mechanical energy and generates a back pressure that opposes to the turbine rotation motion. The back pressure generated in the subsequent bucket "S" for the Thake methodology is consistent with the velocity vectors analyzed in the following section.

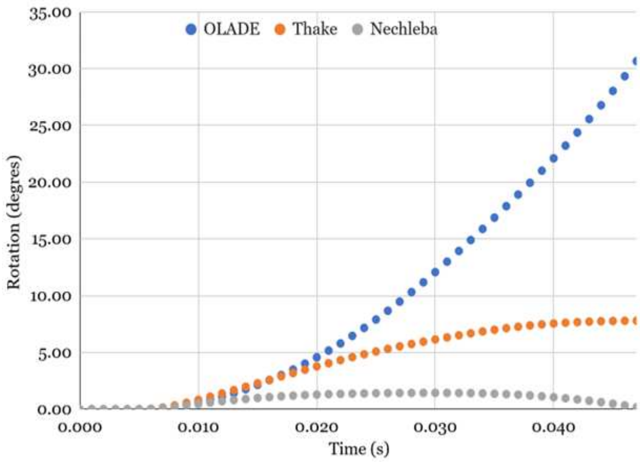


**Fig. 5.** Time behavior of the rotation angle, θ, for the three dimensioning methodologies considered here (OLADE, Nechleba, and Thake).

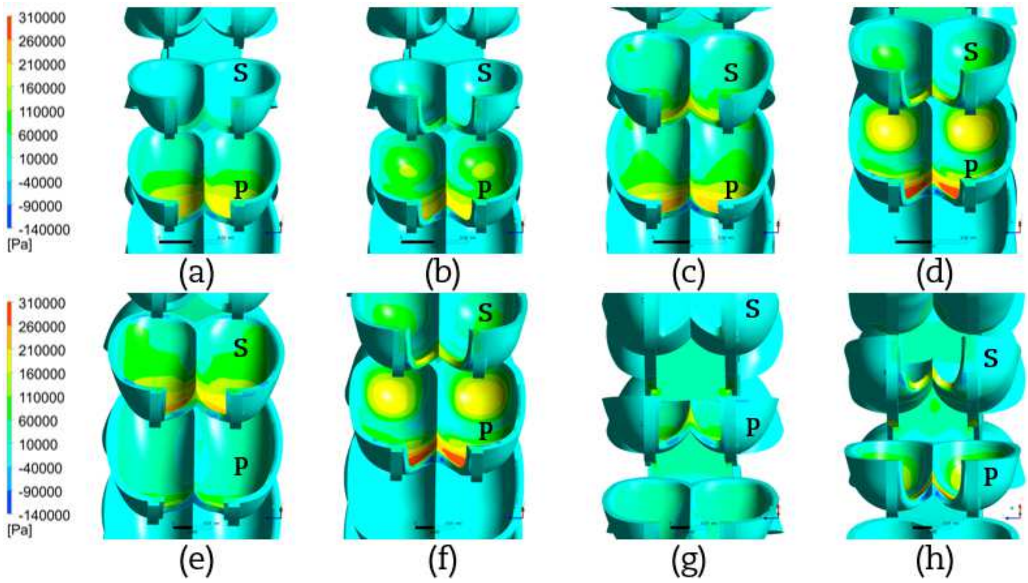


**Fig. 6.** Pressure contours on the buckets' surfaces. (a) OLADE, t = 0 s, θ = 0°, (b) Thake, t = 0 s, θ = 0°, (c) OLADE, t = 2.4 x $10^{-2}$ s, θ = 7.16°, (d) Thake, t = 3.6 x $10^{-2}$ s, θ = 7.14°, (e) OLADE, t = 4.7 x $10^{-2}$ s, θ = 30.65° (Front faces), (f) Thake, t = 4.7 x $10^{-2}$ s, θ = 7.79 (Front faces), (g) OLADE, t = 4.7 x $10^{-2}$ s, θ = 30.65° (Back faces), (h) Thake, t = 4.7 x $10^{-2}$ s, θ = 7.79° (Back faces). Note: Each legend corresponds to the respective row of figures.

### 5.3 Change of fluid momentum by the jet-bucket interaction

The change of the fluid momentum once the jet strikes the turbine is related to the dimension and shapes of the buckets and becomes important to explain the time evolution of the turbine rotation at the first-time instants. In general, the larger the reduction of the magnitude of velocity vectors, the greater the momentum transfer to the buckets, which can boost the turbine rotation. The directions of velocity vectors after the fluid impact are important as well to guarantee the flow spreading far from the back faces of the following buckets, thereby avoiding the generation of reverse torques during the motion. Fig. 7 presents the interaction between the jet and bucket, represented by the fluid velocity vectors at different time-instants for both the OLADE and Thake dimensioning methodologies. At the first time-instant, when the rotation angle for both buckets is $\theta = 0°$ (Fig. 7a,b for OLADE and Fig. 7c,d for Thake), the spread of fluid in the OLADE bucket has a smooth and almost unrestricted exit away from the bucket. The unstable flow patterns on the bucket surface changed over time as the bucket rotates, and the local bucket torque decreases until the water jet flows out of this bucket to the subsequent bucket [18]. On the other hand, in the Thake buckets, a more significant part of the bounced fluid collides with the back face of the subsequent bucket, denoted as "S", which eventually generates a back pressure that decreases the net torque, hindering the rotation movement. Accordingly, energy losses occur when the water jet provides some counter-torque on the bucket's outer side, as was discussed by Nigussie et al. [31]. The adverse influence of the counter-torque is more evident at a time of t = 4.7 x $10^{-2}$ s, where the bucket designed with OLADE methodology has rotated $\theta = 30.65°$, while the bucket designed with Thake methodology has rotated only $\theta = 7.79°$ approximately, as shown in Fig. 7i-l. This behavior can be attributed to the cross-sectional shape of the buckets. The OLADE bucket has a pronounced arc of circumference at the rear part of the cavity, as shown in the images of Table 2, while the shape of the Thake bucket is less smoothed in this part of the cavity, which can lead to an inefficient fluid flow out of the bucket. At the final time-instant, t = 4.70 x $10^{-2}$ s, the concentration of velocity vectors on the rear part of the bucket's cavity, with the consequent lack of flow spreading far from the back surface of the next bucket, is still more evident for Thake than for OLADE.

### 5.4 Pressure contours surrounding fluid

In Fig. 8, pressure contours of the multiphase flow fluid in the symmetry plane of the set runner-bucket are shown for both the OLADE and Thake methodologies. Pressure gradients in the vicinity of the buckets are of particular interest since they can boost or hinder the turbine rotation, as reported by [12]. For the first rotation angles (Fig. 8c,e for OLADE, and Fig. 8d,f for Thake), an important difference is observed between both methodologies: in the Thake methodology, a low pressure zone arises at the right of the bucket struck by the water jet, leading a reverse pressure gradient (opposite to the turbine motion); this is not present in the OLADE methodology for the struck bucket, where the surrounding pressure gradient favors the turbine rotation. For the remaining rotation angles, the condition of reverse pressure gradients persists for Thake, although in lower magnitude. This analysis suggests that the pressure contours shapes around the struck buckets are highly influenced by the dimensioning methodology (OLADE, Thake) and can affect the turbine motion.

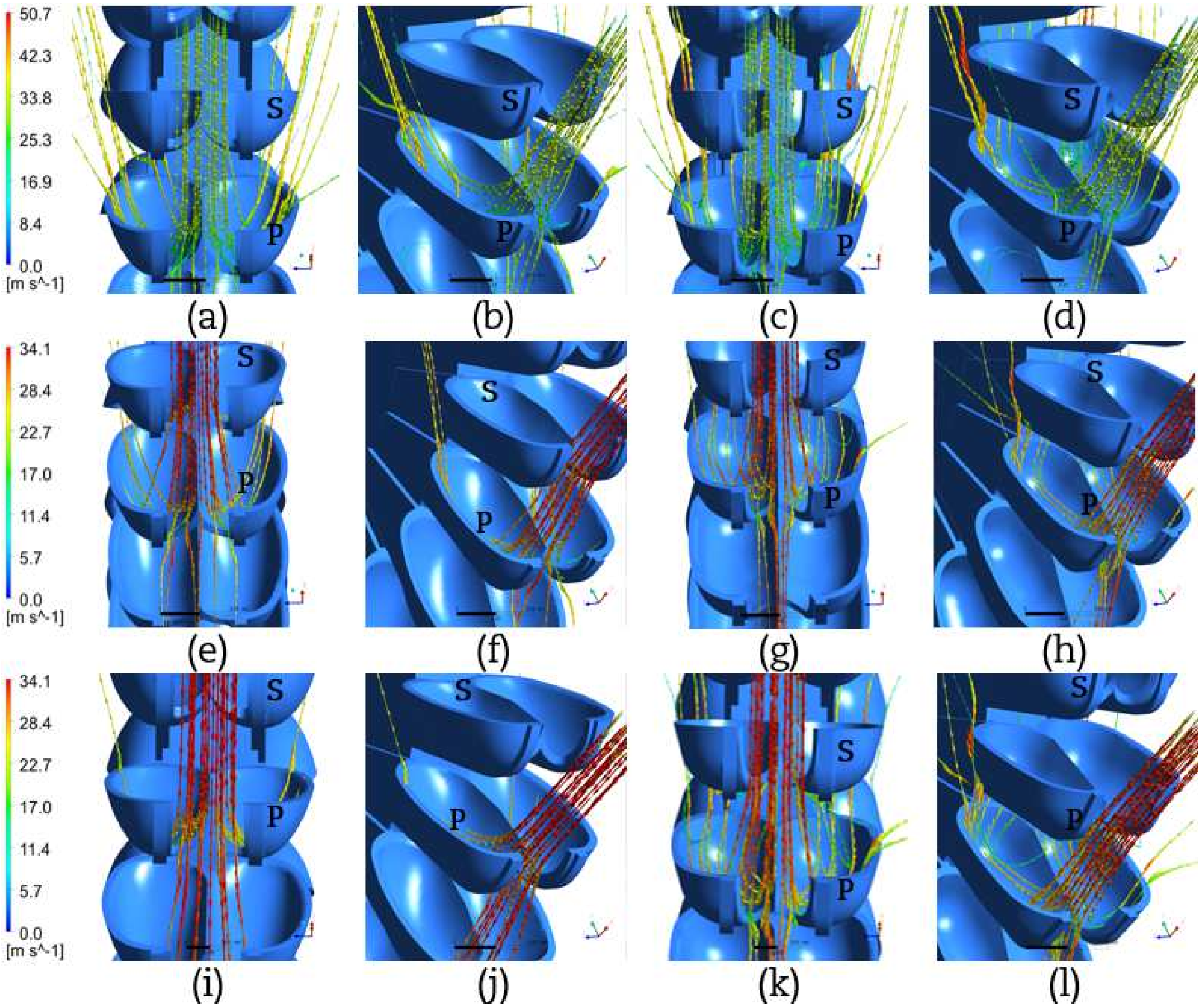


**Fig. 7.** Velocity contours. (a) and (b) OLADE, t = 0 s, θ = 0°, (c) and (d) Thake, t = 0 s, θ = 0°, (e) and (f) OLADE, t = 2.4 x $10^{-2}$ s, θ = 7.16°, (g) and (h) Thake, t = 3.6 x $10^{-2}$ s, θ = 7.14°, (i) and (j) OLADE, t = 4.7 x $10^{-2}$ s, θ = 30.65°, (k) and (l) Thake, t = 4.7 x $10^{-2}$ s, θ = 7.79°. Note: Each legend corresponds to the respective row of figures.

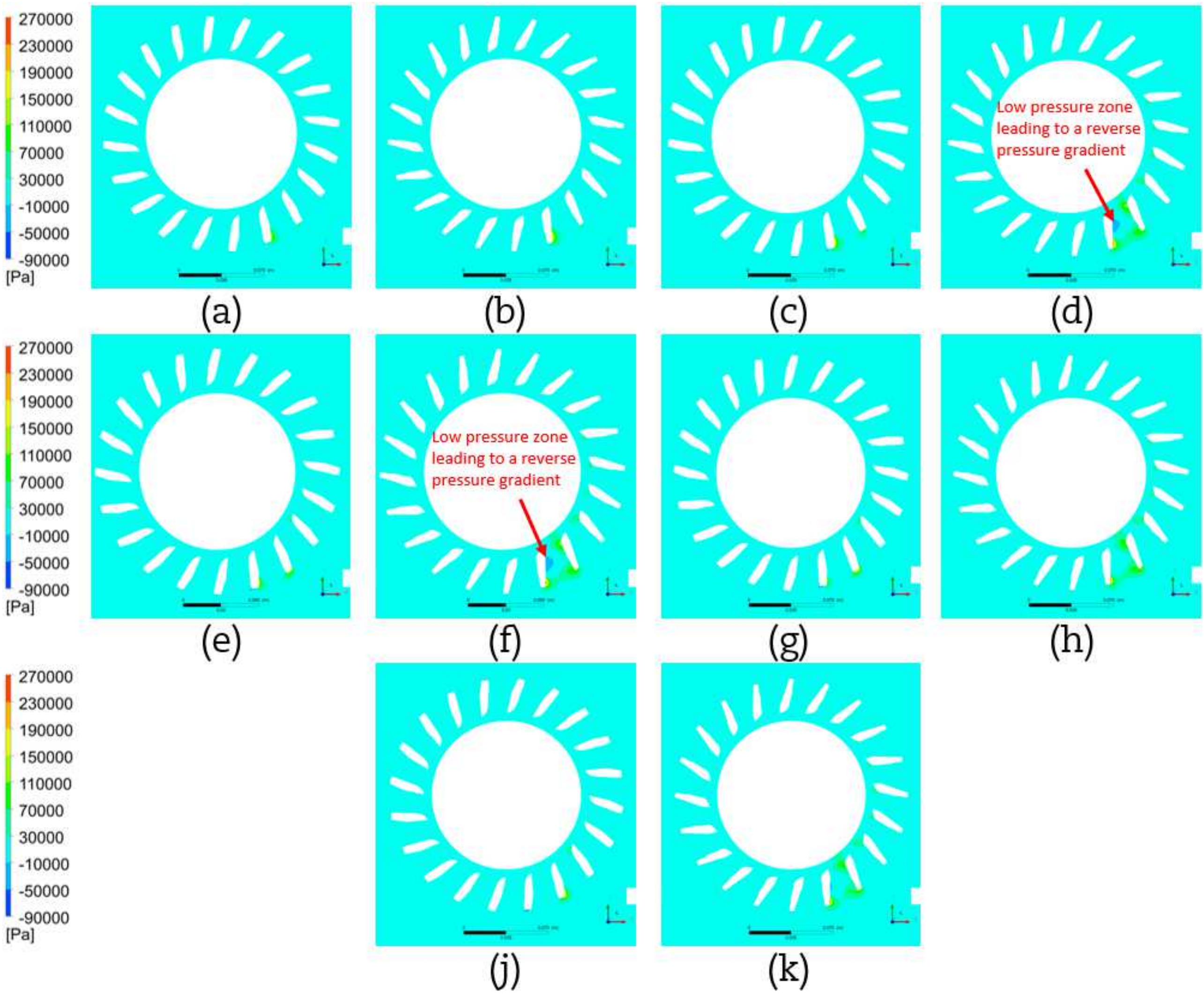


**Fig. 8.** Pressure contours of surrounding fluid. (a) OLADE, t = 0 s, θ = 0°, (b) Thake, t = 0 s, θ = 0°, (c) OLADE, t = 1.5 x $10^{-2}$ s, θ = 2.145°, (d) Thake, t = 1.5 x $10^{-2}$ s, θ = 2.287°, (e) OLADE, t = 2.10 x $10^{-2}$ s, θ = 5.164°, (f) Thake, t = 2.4 x $10^{-2}$ s, θ = 4.841°, (g) OLADE, t = 2.40 x $10^{-2}$ s, θ = 7.161°, (h) Thake, t = 3.60 x $10^{-2}$ s, θ = 7.140°, (i) OLADE, t = 4.70 x $10^{-2}$ s, θ = 30.652° (j) Thake, t = 4.70 x $10^{-2}$ s, θ = 7.779°. Note: Each legend corresponds to the respective row of figures.

## 6. Conclusion

In the present work, multiphase fluid-dynamics simulations were run to evaluate the behavior of Pelton-type turbines at the first-time instants considering three different buckets dimensioning methodologies, namely, OLADE, Nechleba, and Thake. The principal purpose was to assess the ability of each bucket design to overcome a prescribed initial torque of 12.31 N.m under specific operating conditions ($H_g$ = 68 m, $H_n$ = 61.2 m, Q = 4.4 l/s, $n$ = 1800 rpm). According to CFD results, OLADE buckets induce a turbine motion almost 4 times faster than the Thake ones, while the Nechleba buckets could not overcome the initial torque for the operating conditions specified. The geometry of Thake bucket leads to the bifurcated water to be distributed over the entire surfaces of the bucket's cavities, generating important values of pressures in the rear part of these cavities; additionally, for this methodology, an important quantity of streamlines leaving the bucket's cavities collide with the back face of the next bucket, generating a counter-torque on the Pelton-type turbine. These phenomena dampen the turbine rotation, which is globally manifested with a relevant reduction of the angular velocity. On the other hand, the bucket designed with OLADE methodology, given its circumferential arc-type longitudinal profile, favors the spreading of water out of the bucket´s cavities with a lower interference with the back surface of the next bucket; additionally, pressure tends to concentrate on the front part of the cavities in OLADE. These phenomena boost the turbine rotation, generating larger angular velocities.

## Author Contributions

J.M. Ceballos Zuluaga developed the geometrical model, planned the computational scheme, and participated in results analysis. C.A. Isaza Merino researched the State of the Art and participated in results analysis. I.D. Patiño Arcila described the computational model, built computational simulations, and participated in results analysis. A.D. Andrés David Morales Rojas structured the entire manuscript and participated in results analysis. All authors contributed to the writing of the manuscript, discussed the results, reviewed, and approved the final version.

## Acknowledgments

The authors are gratefully acknowledged to the Institución Universitaria Pascual Bravo, Facultad de Ingeniería, Grupo de Investigación e Innovación en Energía (GIIEN), Grupo de Investigación e Innovación Ambiental (GIIAM), and the Dirección de

Tecnología e Innovación for their collaboration in the realization of this project.

## Conflict of Interest

The authors declared no potential conflicts of interest concerning the research, authorship, and publication of this article.

## Funding

This work was supported by the Institución Universitaria Pascual Bravo, Project: “Diseño y fabricación de una pico central eléctrica con turbina tipo Pelton por medio de fundición y mecanizado por control numérico computarizado (CNC)”.

## Data Availability Statements

The datasets generated and/or analyzed during the current study are available from the corresponding author on reasonable request.

## Nomenclature

| | | | |
|---|---|---|---|
| $B$ | Bucket width | $n$ | Angular velocity |
| $C_0$ | Jet velocity | $P_h$ | Hydraulic power |
| $d_0$ | Jet diameter | $Q$ | Water flow rate |
| $D$ | Bucket depth | $T$ | Torque |
| $D_P$ | Runner diameter | $Z$ | Number of buckets |
| $f$ | Notch to jet center distance | $Z_{\min}$ | Minimum number of buckets |
| $g$ | Gravitational acceleration | $Z_{\max}$ | Maximum number of buckets |
| $H_g$ | Gross head | $\beta_1$ | Jet outlet angle at the bucket |
| $H_n$ | Net head | $\beta_2$ | Splitter front angle |
| $k_C$ | Nozzle velocity coefficient | $\eta_h$ | Hydro-efficiency |
| $k_U$ | Speed ratio | $\eta_r$ | Roll efficiency |
| $L$ | Bucket length | $\eta_T$ | Volumetric efficiency |
| $l$ | Bucket height | $\eta_v$ | Total efficiency |
| $M$ | Notch width | $\gamma$ | Specific weight of water |

## References

[1] IEA, Key World Energy Statistics 2021 – Analysis, IEA, septiembre de 2021. https://www.iea.org/reports/key-world-energy-statistics-2021 (accedido 8 de octubre de 2022).
[2] UPME, Boletín estadístico de Minas y Energía, 2019. https://www1.upme.gov.co/Hemeroteca/Paginas/Boletin-estadistico-de-ME.aspx (accedido 8 de octubre de 2022).
[3] European Renewable Energy Council, Renewable Energy in Europe Markets, Trends and Technologies, 2015.
[4] Keck H., Sick M., Thirty years of numerical flow simulation in hydraulic turbomachines, *Acta Mechanica*, 201, 2008, 211-229.
[5] Židonis A., Aggidis G.A., State of the art in numerical modelling of Pelton turbines, *Renewable and Sustainable Energy Reviews*, 45, 2015, 135-144.
[6] Nechleba M., Hydraulic turbines: their design and equipment, 1957.
[7] Mosonyi E., Water Power Development, 2 High-head power plants A, 1991.
[8] Eisering M., Micro Pelton Turbines Harnessing Water Power on a Small Scale - Element 9, 1991, Accedido: 24 de septiembre de 2022.
[9] Thake J., *Micro-hydro Pelton Turbine Manual*, PRACTICAL ACTION PUBLISHING, 2000.
[10] Solemslie B.W., Dahlhaug O.G., A reference Pelton turbine design, *IOP Conference Series: Earth and Environmental Science*, 15(3), 2012, 032005.
[11] Židonis A., Aggidis G.A., Pelton turbine: Identifying the optimum number of buckets using CFD, *Journal of Hydrodynamics, Ser. B*, 28, 2016, 75-83.
[12] Židonis A., Panagiotopoulos A., Aggidis G.A., Anagnostopoulos J.S., Papantonis D.E., Parametric optimisation of two Pelton turbine runner designs using CFD, *Journal of Hydrodynamics, Ser. B*, 27, 2015, 403-412.
[13] Ceballos Zuluaga J.M., Isaza Merino C.A., Patiño Arcila I.D., Morales Rojas A.D., Análisis comparativo de las metodologías de dimensionamiento de cangilones para turbinas Pelton en sistemas de micro-generación, *INGENIERÍA Y COMPETITIVIDAD*, 25, 2023, doi: 10.25100/iyc.v25i1.11797.
[14] Avellan F., Dupont P., Kvicinsky S., Chapuis L., Parkinson E., Vullioud G., Flow Calculations in Pelton Turbines. Part 2: Free Surface Flows, *Proceedings of the19th IAHR Symposium on Hydraulic machinery and cavitation*, Singapore, Republic of Singapore, 1998.
[15] Zoppé B., Pellone C., Maitre T., Leroy P., Flow analysis inside a Pelton turbine bucket, *Journal of Turbomachinery*, 128, 2006, 500-511.
[16] Klemetsen L.E., *An experimental and numerical study of the free surface Pelton bucket flow*, Master Thesis, Norwegian University of Science and Technology, 2010.
[17] Perrig A., Avellan F., Kueny J.L., Farhat M., Parkinson E., Flow in a Pelton turbine bucket: Numerical and experimental investigations, *Journal of Fluids Engineering, Transactions of the ASME*, 128, 2006, 350-358.
[18] Xiao Y.X., Cui T., Wang Z.W., Yan Z.G., Numerical simulation of unsteady free surface flow and dynamic performance for a Pelton turbine, *IOP Conference Series: Earth and Environmental Science*, 15, 2012, 052033.
[19] Zeng C., et al., Hydraulic performance prediction of a prototype four-nozzle Pelton turbine by entire flow path simulation, *Renewable Energy*, 125, 2018, 270-282.
[20] Parkinson E., Vullioud G., Geppert L., Keck H., Analysis of Pelton turbine flow patterns for improved runner-component interaction, *International Journal on Hydropower & Dams*, 9, 2002, 100-103.
[21] Hana M., A Discussion on Numerical Simulation in Pelton Turbines, *Proc. 19th IAHR Symp.*, Singapore: World Scientific, 1998.
[22] Kvicinsky S., Kueny J.L., Avellan F., Parkinson E., Experimental and Numerical Analysis of Free Surface Flows in a Rotating Bucket, *Proc. XXIst IAHR Symp. Hydraul. Mach. Syst. Lausanne: Laboratory for Hydraulic Machines*, 2002.
[23] Anagnostopoulos J.S., Papantonis D.E., A Fast Lagrangian Simulation Method for Flow Analysis and Runner Design in Pelton Turbines, *Journal of Hydrodynamics*, 24, 2012, 930-941.
[24] Vessaz C., Andolfatto L., Avellan F., Tournier C., *Toward design optimization of a Pelton turbine runner*, 2017.
[25] Coz F., et al., *Manual de mini y microcentrales hidráulicas*, Lima, 1995.
[26] Hernandez C., *Indacochea E., Apuntes para un diseño, estandarizacion y fabricación de equipos para pequeñas centrales hidroelectricas*, Volumen II, Turbinas Pelton, Lima, 1988.
[27] ANSYS INC, Lecture 7: Course of Introduction to ANSYS Meshing. In Course os Introduction to ANSYS Meshing, 2015.
[28] ANSYS INC, Appendix A: Mesh Quality. In Training Manual: ANSYS Meshing Application Introduction, 2009.
[29] Zeng Y., Wang J., Ding S., Zhou H., Zang Y., Li F., Simulation Study on Dynamics of Hydraulic Turbines Used in Drilling Engineering, *Shock and Vibration*, 2020, 2020, 1-14.
[30] Panthee A., Neopane H.P., Thapa B., CFD Analysis of Pelton Runner, *International Journal of Scientific and Research Publications*, 4, 2014, 50-55.

[31] Nigussie T., Engeda A., Dribssa E., Design, Modeling, and CFD Analysis of a Micro Hydro Pelton Turbine Runner: For the Case of Selected Site in Ethiopia, *International Journal of Rotating Machinery*, 2017, 2017, e3030217.

## ORCID iD

Jorge Mario Ceballos Zuluaga https://orcid.org/0000-0002-0781-2875
Cesar Augusto Isaza Merino https://orcid.org/0000-0001-6632-9691
Iván David Patiño Arcila https://orcid.org/0000-0002-2876-8930
Andrés David Morales Rojas https://orcid.org/0000-0003-2876-8719



**How to cite this article:** Ceballos Zuluaga J.M., Isaza Merino C.A., Patiño Arcila I.D., Morales Rojas A.D. Fluid-dynamic Simulations for Assessment of Dimensioning Methodologies of Pelton Turbine Buckets Considering the Initial Torque Overcoming, *J. Appl. Comput. Mech.*, 9(4), 2023, 1036–1048. https://doi.org/10.22055/jacm.2023.42512.3935